# Robust amphiprotic Konjac Glucomannan Cross-linked Chitosan Aerogels for Efficient Water Remediation

**Jiajun Mao[a] · Shuhui Li[a,b] · Chenglin He[c] · Yuxin Tang[d] · Zhong Chen[e] · Jianying Huang[a*] · Yuekun Lai[a,c*]**

[a] College of Chemical Engineering, Fuzhou University, Fuzhou 350116, P. R. China

[b] Department of Chemistry, University College London, London, UK

[c] National Engineering Laboratory for Modern Silk, College of Textile and Clothing Engineering, Soochow University, Suzhou 215123, P. R. China

[d] Institute of Applied Physics and Materials Engineering, University of Macau, Macau, P. R. China

[e] School of Materials Science and Engineering, Nanyang Technological University, 50 Nanyang Avenue, Singapore

[*]Corresponding author

Corresponding author email: jyhuang@fzu.edu.cn; yklai@suda.edu.cn

**Abstract**

Robust amphiprotic-konjac glucomannan/chitosan (AP-KGM/CS) aerogels were prepared by modification of KGM with carboxymethyl and quaternary ammonium groups, and then cross-linked with chitosan. The adsorption performance of AP-KGM/CS aerogels on the anionic dyes everacid Orange N-G (C.I. Acid Orange O56), cationic dyes methylene blue (MB) and heavy metal ions ($Pb^{2+}$, $Cu^{2+}$, $Cd^{2+}$) were investigated. The open porous structure of the aerogel has a significant effect on maintaining the structural stability of aerogel and promoting the diffusion and transfer of pollutants to ensure adequate contact between pollutants and adsorption sites. The adsorption equilibrium of anionic dye O56 and cationic dye MB was reached within 300 min, and the saturated adsorption capacities were 267 mg/g and 348 mg/g, respectively. Besides, the adsorption equilibrium of single metal ions $Pb^{2+}$, $Cu^{2+}$, and $Cd^{2+}$ was reached within 120 min, and their saturated adsorption capacities were 469 mg/g, 254 mg/g and 144 mg/g, respectively. Moreover, under the competitive adsorption of three heavy metal ions, the equilibrium adsorption time of $Pb^{2+}$, $Cu^{2+}$, and $Cd^{2+}$ in the mixed solutions (each with a concentration of 600 mg/L) was 240 min, 150 min and 70 min, respectively, and their saturated adsorption capacities were 318 mg/g, 184 mg/g and 94 mg/g, respectively.

**Keywords:** Konjac Glucomannan; Chitosan; Hybrid Aerogels; Heavy metal ions removal; Dye absorption

## Introduction

Water is of major importance to the survival and development of human society. Water pollution has become a serious problem since the industrialization began in the 18$^{th}$ century. Currently, shortage of clean water has become a global crisis and the problem keeps worsening (Ahmad and Danish, 2018). Among different types of water pollutants, heavy metal contamination is mainly caused by indiscriminate discharge of industrial waste water, which brings direct or indirect hazards to the human living environment (Bacelo et al. 2016; Chuah et al. 2005; Ngah et al. 2011; Tang et al. 2010; Zhang et al. 2016). Heavy metal ions are mainly from the mining, metallurgy, chemical, electronics, leather, paper and other industries. The excessive dependence on coal, oil and other fuels, chemical fertilizers, pesticides has worsened the problems related to heavy metal contamination. Metal ions are very stable in water, and are not easily degraded by biological methods. In some cases, they may even be converted into more toxic chemical form, causing serious harm to biological and human health (Zhao et al. 2010). The pollutants manifested as a long-term damage to the biological nervous system, the digestive system, urinary system cells, organs, skin and bone; its consequences and effects are extremely serious and far-reaching (Kim et al. 2012). Therefore, heavy metal pollution has become one of the most serious environmental problems in the world and the treatment of heavy metal wastewater has attracted much attention in recent years(Aragay et al. 2011; Ge et al. 2018; Li et al. 2019).

In order to effectively remove these heavy metal ions, a variety of remedial techniques have been developed, including ion exchange, coagulation sedimentation,

membrane filtration, reverse osmosis, adsorption and so on (Bethke et al. 2018; Hu et al. 2008; Liu et al. 2017; Miao et al. 2017). Among them, adsorption technology is one of the most promising strategies due to its wide range of adaptability, ease of handling, relatively low cost and the availability of different adsorbents (Liu et al. 2019; Wu and Zhao 2011). Various adsorbents have been studied for the removal of heavy metal contaminants from aqueous solutions, including activated carbon, zeolites, minerals (clays), molecular sieves, and other inorganic nanomaterials (Ding et al. 2016; Mao et al. 2017; Wang et al. 2016). However, these adsorbents generally have a low removal ability, slow capture ability, separation difficulties, secondary environmental pollution, and poor recoverability, which greatly hamper their practical application. To improve the efficiency of the wastewater treatment process, new adsorbent materials are needed that are environmentally friendly, efficient and inexpensive (Liu et al. 2018). Such necessity becomes increasingly urgent as the environmental pollution problems become more and more serious in recent year (Dehghani et al. 2016; Tahmasebi et al. 2015). Modified adsorbents, based on modification of a wide range of raw materials, are able to offer several advantages such as low prices, good reproducibility and biodegradability, therefore they represent a promising direction for the development of adsorbent materials (Zhang et al., 2017). Konjac Glucomannan (KGM) is a natural polymer, which is abundant, low cost, and possesses good adsorption capacity. It has been used in various ways to construct composite aerogel adsorbents recently (Si et al. 2016; You et al. 2018).

KGM is a high molecular weight water-soluble non-ionic polysaccharide that is linked by D-glucose and D-mannose at a molar ratio of 1: 1.5 to 1.7 and β-1, 4 and β-1, 3 glycosidic bonds (Katsuraya et al. 2003). Compared with other polysaccharide compounds, KGM has been widely used in food, packaging, coatings, biomedical field due to its attractive physical and chemical properties (Chen et al. 2017). However, natural KGM has the disadvantages of poor rheology, poor stability in aqueous solution, easy degradation and short storage life. KGM microspheres are formed under near-neutral conditions and would rapidly expand in water. All these shortcomings have limited its wide application. In order to improve the physical and biological properties of KGM, certain methods have been used to modify KGM (Wang et al. 2011). Some researchers have grafted the functional groups on KGM for absorption of tannins, copper, lead, cadmium and other heavy metal ions in water (Huang et al. 2011). There are also some reports on the preparation of in vitro antibacterial materials based on modified KGM (Zhu et al. 2015).

Based the above discussion, there exists a need for low cost, high performance and recyclable adsorbents. Therefore, it is of great theoretical and practical significance to develop advanced adsorbents that are effective and easy to regenerate or dispose. A high performance adsorbent should have a large specific surface area, enrichment of functional groups and porous structure (Werber et al. 2016). In order to meet these requirements, we have designed and prepared new KGM aerogels with extremely high density of carboxyl and amino bifunctional groups.

## Experimental section

**Materials:** KGM (viscosity ≥ 15000 mpa.s) was provided by Suzhou Branch of Biological Technology Co., Ltd. Isopropanol, Copper (II) chloride dehydrate, Lead chloride, Cadmium chloride and NaOH were provided by Jiangsu powerful functional Chemical Co., Ltd. Chloroacetic Acid was provided by Shanghai Titan Technology Co., Ltd. 3-Chloro-2-hydroxypropyltrimethylammonium Chloride was purchased from Suzhou Branch with the biomedical Technology Co., Ltd. HCl (36-38%) was obtained from Soochow University experimental material supply center. Ethanol was provided by Jiangsu powerful functional Chemical Co., Ltd. Acid dyes everacid Orange N-G (C.I. Acid Orange 56) was obtained from Everlight Chemical Industry, Taiwan. Methylene Blue was purchased from Sinopharm Chemical Reagent Co., Ltd. All chemical reagents are analytical-grade and used as received without further purification.

**Preparation of CMKGM:** 15 g of KGM and 50 mL of Isopropyl alcohol were put into a three-necked flask equipped with a stirrer and a condensing unit, and 12 mL of 45% aqueous solution of sodium hydroxide was added gradually while stirring at 50°C, and then the mixture was stirred for 2 h. After 12 mL of 80% monochloriacetic acid was added, the mixture was continuously stirred for 4 h and then filtered. The filtrate was washed with 60, 70, 80 and 100 wt% 15 mL ethanol solutions consecutively to remove impurities. The filtrate was vacuum-dried at 60°C and milled to get the desired CMKGM.

**Preparation of CTA-CMKGM:** 10 g of CMKGM and 50 mL of isopropanol was placed in a three-necked flask equipped with a stirrer and a condensing unit, and 5 mL of 45% sodium hydroxide aqueous solution was gradually added while stirring at 50 °C,

and the mixture was stirred for 1 h. Then 16 mL of 60% 3-chloro-2-hydroxypropyltrimethylammonium chloride solution was added and the mixture was stirred continuously for 3 hours and then filtered. The filtrate was washed with 60%, 70%, 80% and 100 wt% 15 mL ethanol solutions consecutively until the solution was neutral. The filtrate was dried in a vacuum oven at 60°C for 12 h and ground to obtain the desired CTA-CMKGM.

**Preparation of amphiprotic KGM aerogels:** 1.4 g of AP-KGM was dispersed in 25 mL of deionized water while 0.6 g of chitosan was added to 25 mL of glacial acetic acid solution (4 wt.%). The dissolved chitosan solution was then added slowly to obtain AP-KGM dispersion, and the mixture was added into a concentration of 2.5% (Huang et al. 2018) glutaraldehyde solution. After that, the solution was stirred for a period of time and reacted at 50°C water bath for 1 h to make it cross-linked. Finally it was placed into a cryogenic freezer refrigerator (-80°C) frozen for 4 h to obtain the AP-KGM/CS aerogels.

**Adsorption of dyes and monometal ions:** The adsorption of amphiprotic KGM aerogel (100 mg) to dyes and metal ions with contacting time from 10 to 600 min was investigated. The initial concentration of metal ions is 200 mg/L and the test was carried out at room temperature. The effect of concentration (25-1000 mg/L) was investigated with the same amount of adsorbent. The adsorption capacity $Q_e$ (mg/g) was determined according to the equation (1):

$$Q_e = (C_0 - C_t) \times V/m \quad (1)$$

where $C_0$ (mg/L) is the initial solution concentration, and $C_t$ is the solution concentration at time t, V (L) is the volume of solution and m (g) is the mass of adsorbents.

**Multiple metal ions competitive adsorption experiment:** Multiple metal ions competitive adsorption experiment was performed by following the same procedure with the monometal experiment. Specifically, the adsorption capacity was investigated in a range from 10 to 600 min using 100 mg of aerogel as adsorbent. The initial concentration of each metal ions was 600 mg/L, and experiment was carried out at room temperature.

**Characterization:** Fourier transform infrared (FTIR) spectra were recorded on a Nicolet 5700 Fourier transform infrared spectrophotometer equipped with a single reflection attenuated total reflectance (ATR) system at a scan range of 4000-400 $cm^{-1}$. The microstructure and elemental information of the aerogels were investigated using a TM3030 scanning electron microscopy equipped with an energy-dispersive X-ray spectroscope (EDX). A Kratos Axis-Ultra HSA X-ray photoelectron spectrometer (XPS) was used to examine the chemical composition with a 100 W AlKα X-ray source and a base pressure of $4 \times 10^{-9}$ mbar. The concentrations of metal ions were measured using a Thermo Scientific ICAP 6000 DUO inductively coupled plasma atomic emission spectroscopy. The UV-vis spectra was recorded on a UV-Vis-NIR Spectrophotometer (Cary 5000, Agilent) at room temperature with a wavelength range from 200 to 800 $cm^{-1}$. The concentration of dye was determined according to the maximum absorbance of the solutions.

## Results and discussion

Herein, we report a novel amphiprotic carboxymethyl Konjac Glucomannan/chitosan (KGM/CS) hybrid aerogel with a 3D intensive network, utilizing the modified Konjac Glucomannan cross-linked with chitosan (Fig. 1). Cationic carboxyl groups and anionic quaternary ammonium groups were grafted onto KGM to obtain high-performance adsorbent for water remediation application. In addition, chitosan could strengthen the mechanical strength as well as hydrophilicity of the functional KGM frameworks (Plamper F A and W Richtering, 2017).

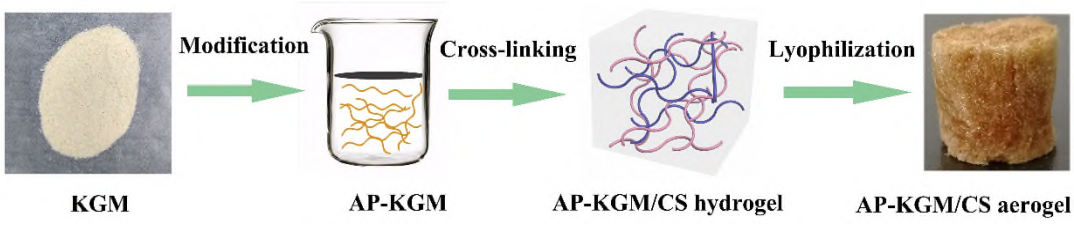


**Figure 1.** Schematic illustration of the synthesis of AP-KGM/CS aerogel.

The microscopic morphology of KGM powder presented a smooth surface with a few wrinkles (Fig. S1 a-c). Fig. S1 (d-f) show the surface morphology of konjac glucomannan after carboxymethylation modification. A large number of micro-nano pores were uniformly distributed on the surface. With further grafting of CTA, the surface of the as-synthesized AP-KGM was rougher, and more micropores and nanopores appeared, which has resulted in the increases of specific surface area (Fig. S1 g-i). By cross-linking AP-KGM with chitosan and a 3D AP-KGM/CS aerogel was synthesized, it can be found that such a cylindric aerogel can easily stand on the top of dandelion due to its light weight (Fig. 2a). Fig. 2b-e show SEM pictures of the as-

prepared AP-KGM/CS aerogels with mass ratios (AP-KGM/CS) of 5:5, 6:4, 7:3, and 8:2. These aerogels showed a three-dimensional highly porous network structure, and with the increase of AP-KGM component, the pore size of aerogel increased gradually. When the mass ratio of AP-KGM/CS was 7:3, the pore size of AP-KGM/CS aerogel was uniform, constructing a higher porous network.

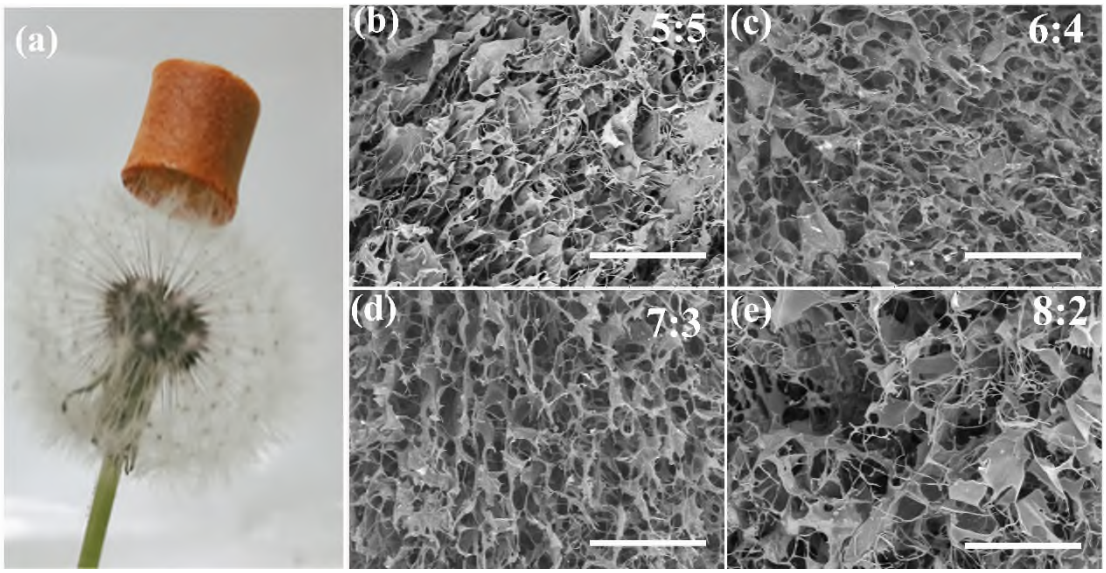


**Figure 2.** (a) Optical picture of AP-KGM/CS aerogel standing on the top of dandelion. (b-e) SEM images on the AP-KGM/CS aerogels with different mass raios. Scale bar is 200 μm.

Fig. 3a shows the FT-IR spectra of AP-KGM, CS, and AP-KGM/CS aerogels. AP-KGM showed a C-N vibration peak at 1320 $cm^{-1}$, which indicates that the quaternary ammonium group had been grafted onto CM-KGM. After the chitosan was introduced, characteristic absorption peaks of amide I band (σC=O) and amide II band (δN-H) at 1638 $cm^{-1}$ and 1563 $cm^{-1}$ was observed from CS and AP-KGM/CS aerogel, respectively (Pillai et al. 2009). Fig. S2 shows the FT-IR spectra of the KGM, CM-KGM and the

AP-KGM. Compared with the C=O stretching vibrations of KGM at 1650 $cm^{-1}$, the C=O band of CM-KGM shifted to 1602 $cm^{-1}$ corresponding to the carboxyl group (-COO). Moreover, the peak of carboxyl group (-COO-) appeared at 1420 $cm^{-1}$, suggesting that the carboxymethyl group was grafted onto KGM.

The elemental state of CTA/CM-KGM was further analyzed by X-ray photoelectron spectroscopy. Fig. 3b-d show the high-resolution electron spectra C1s of CM-KGM and AP-KGM, AP-KGM/CS. Compared with CM-KGM, the XPS spectrum of AP-KGM showed a new peak at 285.5 eV corresponding to C-N bands, indicating that CTA was grafted onto konjac glucomannan. After the hybridization with the CS, intensity of C-O peak decreased and C-N peak increased significantly. This indicates that AP-KGM has been successfully linked with CS and formed a stable network.

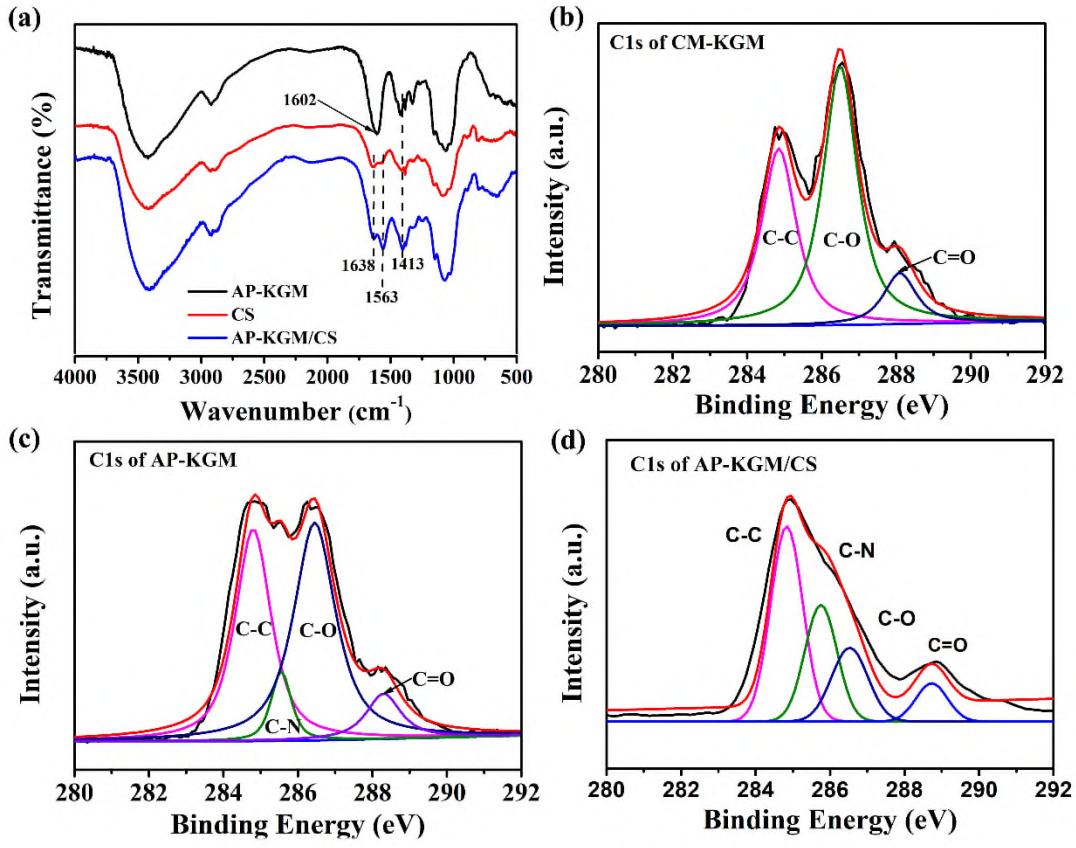

**Figure 3.** (a) FT-IR spectra of AP-KGM, CS, AP-KGM/CS. High resolution C1s spectrum of (b) CM-KGM, (c) AP-KGM, and (d) AP-KGM/CS.

Fig. 4a shows the compressive strength of AP-KGM/CS aerogels at different mass ratios. The compressive strength of AP-KGM/CS aerogel firstly increased and then decreased slightly. When the mass ratio of AP-KGM/CS is 7:3, the compressive strength of the corresponding aerogel reaches the maximum (5.2 kPa). This is because AP-KGM is used as a framework material in the preparation of aerogel, and chitosan plays a role in the shaping. AP-KGM with higher strength can improve the mechanical strength of aerogel, when the mass ratio of KGM/CS reached 8:2, the amount of chitosan was too small, resulting in poor formability of the aerogel and decreased connection of the networks. The AP-KGM/CS aerogels were immersed into wastewater and the hydrogels can still maintain 3D network as well as the porous structure after stirring in water for one week (Figure 4d). Long-chain molecules of AP-KGM were intertwined due to the presence of chitosan that has endowed the double framework with good adhesion. This has ensured the hydrogels with a high integrity and can withstand the shearing force in water (Dai et al. 2015).

Fig. 4b shows the thermogravimetric curves of KGM, CS, AP-KGM and AP-KGM/CS aerogels. There was a minor weight loss below 250 °C, mainly due to evaporation of the surface-adsorbed water. The rapid decomposition temperatures occurred at approximately 360 °C, 352 °C, 340 °C and 336 °C, respectively. Thus the initial thermal stability of chitosan is the best. At 600 °C, the residues of KGM, CS, AP-KGM and AP-KGM/CS aerogel were about 16.1%, 36.7%, 25.6% and 27.2%,

respectively. The thermal stability of KGM has been greatly improved after the chemical modification, and the thermal stability of AP-KGM/CS aerogel with chitosan cross-linked was further improved.

The pH value has a great influence on the adsorption capacity of the adsorbent. Different pH values lead to protonation or deprotonation of the adsorbent surface and thereby change the surface electrical properties of the adsorbent as well as affect its adsorption performance (Yu et al. 2017). The isoelectric points of AP-KGM hydrogels occurred when the pH of water solution was adjusted to 4.1 (Fig. 4c). The surfaces of the hybrid hydrogels are negatively charges as a result of the ionization of oxygen-containing groups when pH > 4.1. The as-prepared hydrogels would have better adsorption ability of metal ions in alkaline conditions.

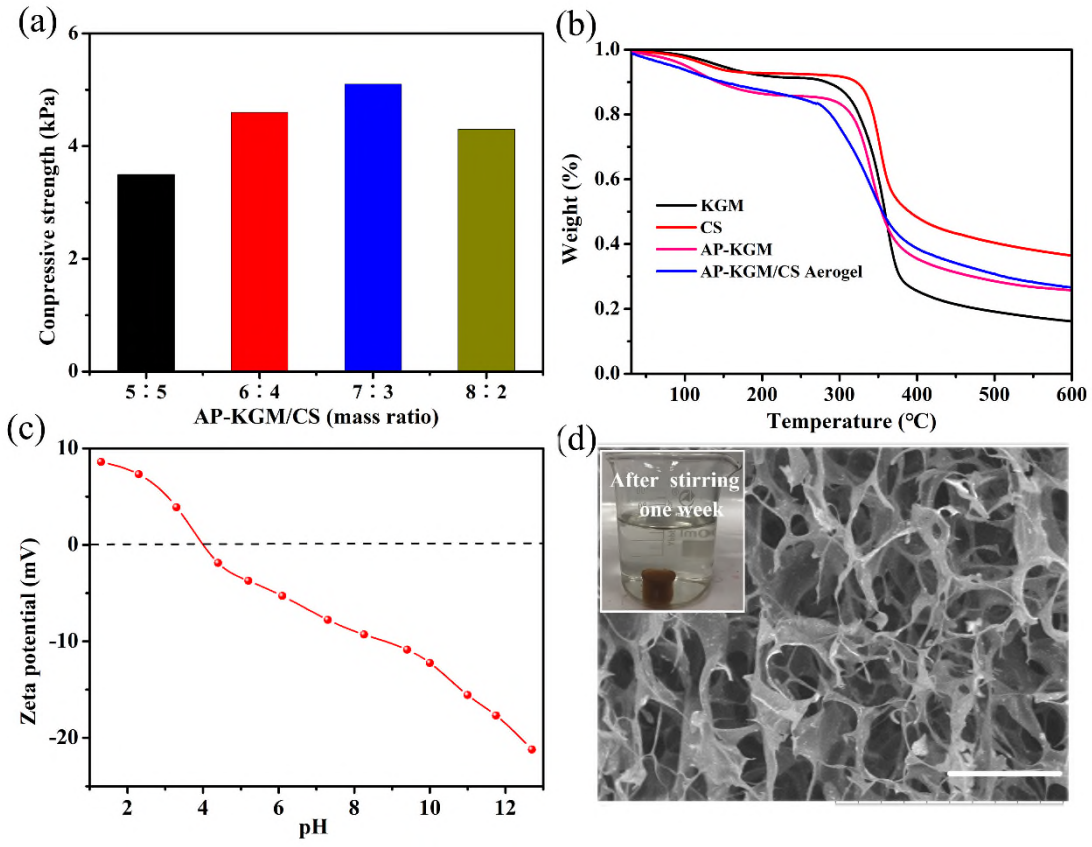

**Figure 4.** (a) Compression strength of the aerogels under diverse mass ratios. (b) Normalized remaining mass of KGM, CS, AP-KGM, and AP-KGM/CS. (c) Zeta potential of AP-KGM/CS as a function of pH values. (d) The morphology of AP-KGM/CS after stirring one week, scale bar is 100 μm.

To demonstrate the effect of pH value on the adsorption performance of $Pb^{2+}$, $Cu^{2+}$ and $Cd^{2+}$ onto AP-KGM/CS, we carried a series of adsorption tests with the same initial concentrations under treatment with 8 h and pH values of pollution solution were adjusted from 2.0 to 6.0. As shown in the Fig. 5a, the adsorption of $Pb^{2+}$, $Cu^{2+}$ and $Cd^{2+}$ increased with increased pH value in general. This is because in the pollution solution of a lower pH, the surface adsorption sites on the adsorbent are mainly occupied by hydronium ions, the concentration of hydronium ions decreased with the increase of pH, and the coulomb repulsion between adsorbed heavy metal ions and hydronium ions decreased (Zhu et al. 2015). Therefore, the adsorption performance gradually increased with increasing pH. In addition, Fig. 5d shows the changes on the adsorption of the dyes O56 and MB by the AP-KGM/CS aerogel when the pH of the solution gradually increased from 2 to 12. Among them, the adsorption of dye O56 by AP-KGM/CS aerogel increased rapidly when the pH was from 2 to 5: the maximum capacity reached was 312 mg/g when pH was around 5. However, as the pH increased further from 5 to 12, the amount of the O56 adsorbed onto AP-KGM/CS aerogel continued to decrease. The main reason lies with the protonation and deprotonation of the adsorbent and the surface active groups of the contaminants. Dye O56 exists as an anion in an acidic environment and as a cation in an alkaline environment. The hydronium ion is greatly

reduced when pH was less than 5, and the adsorption sites on the surface of the adsorbent were greatly increased, which promoted the adsorption of O56. On the other hand, when the pH value was increased from 5 to 12, the surface gradually became negatively charged. The surface of the adsorbent was occupied by a large amount of OH-, and electrostatic repulsion with the dye caused a decreased adsorption amount. In general, the adsorption ability of AP-KGM/chitosan is comparable to that of many aerogel-based adsorbents reported previously (Table S1). As shown in figure S3, there was no obvious morphological changes after metal ions absorption and separation.

Adsorption kinetics is an important part of the adsorption process. It reflects the time required for the adsorbent to reach the adsorption equilibrium (Crini G and P M Badot, 2008). Fig. 5b shows the adsorption of heavy metal ions as a function of time by AP-KGM/CS aerogel. The adsorption of $Pb^{2+}$, $Cu^{2+}$ and $Cd^{2+}$ reached the adsorption equilibrium within 120 min. Fig. 5e shows the adsorption of dyes as a function of time by AP-KGM/CS aerogel. The adsorption equilibrium of dyes O56 and MB was achieved within 300 min. The adsorption efficiency of AP-KGM/CS aerogel for heavy metal ions was significantly higher than that for dyes, mainly because the dye molecules are macromolecules and are much larger than that of metal ions, thus a lower diffusion rates. The adsorption curves of metal ions and dyes fit well with a pseudo-first order kinetic model:

$$\ln (q_e - q_t) = \ln (q_e) - k_1 t \qquad (2)$$

where $Q_e$ (mg/g) represents the equilibrium adsorption capacity of the adsorbent, $Q_t$ (mg/g) the adsorption amount at the time t (min), $k_1$ ($min^{-1}$) the rate constant of the

second-order kinetic equation. The correlation coefficients ($R^2$) of the fits are close to 1.

The equilibrium adsorption isotherm is used to analyze the type of interaction between the adsorbent and the adsorbate. Fig. 5b and 5e show the saturated adsorption of $Pb^{2+}$, $Cu^{2+}$, $Cd^{2+}$, O56 and MB in AP-KGM/CS aerogels with different concentrations of contaminants when pH = 6. In the initial stage, the saturated adsorption capacity of AP-KGM/CS aerogel for heavy metal ions and dyes increased remarkably with the initial concentration of the pollutant solution, and then approached to the equilibrium state with the increases of initial concentration of the pollutant solution. The Langmuir isotherm model is adopted to fit with the experimental data:

$$1/Q_e = (1/bQ_{max})(1/C_e) + 1/Q_{max} \quad (3)$$

where $C_e$ (mg/L), $Q_e$ (mg/g), $Q_{max}$ (mg/g), b (L/mg) are the concentration of pollutants, the amount of adsorption at the equilibrium, the maximum adsorption, and the Langmuir constant that represents the energy of the adsorption process, respectively. In the Langmuir model, the adsorption sites on the surface of the adsorbent are uniformly distributed as a single layer, and the adsorbed substances do not interfere with each other (Ho et al. 2002).

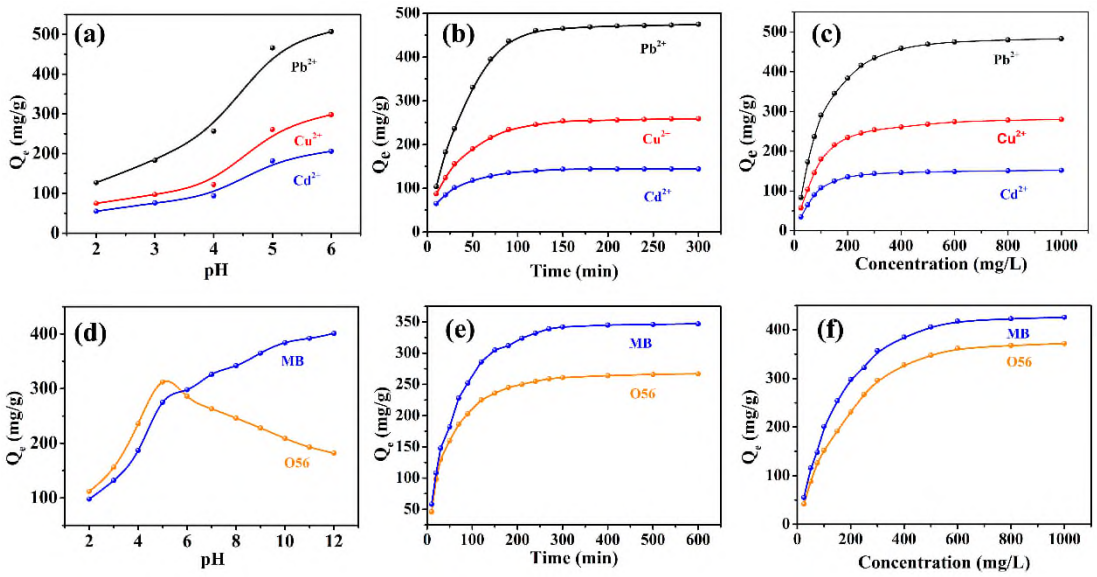


**Figure. 5.** (a, d) The adsorption capacity of $Pb^{2+}$, $Cu^{2+}$, $Cd^{2+}$, MB, and O56 of AP-KGM/CS under different pH values. (b, e) Adsorption isotherm curves of $Pb^{2+}$, $Cu^{2+}$, $Cd^{2+}$, MB, and O56 of AP-KGM/CS, (c, f) Adsorption kinetics of $Pb^{2+}$, $Cu^{2+}$, $Cd^{2+}$, MB, and O56 of AP-KGM/CS as a function of concentration.

To further investigate the roles played by AP-KGM and CS on the adsorption of anionic dyes and heavy metal ions, we prepared AP-KGM/CS aerogel with different mass ratios for the adsorption of the anionic dye acid orange, cationic dye methylene blue (MB) and heavy metal ions ($Pb^{2+}$, $Cu^{2+}$, $Cd^{2+}$) solutions. The adsorption capacity of the AP-KGM/CS aerogel for organic dyes and heavy metal ions at different mass ratios showed different trends (Fig. 6a). With the increases of the AP-KGM content, the complexation between carboxyl groups and heavy metal ions was enhanced, leading to increase adsorption capacity of heavy metal ions by the AP-KGM/CS aerogel. When the mass ratio of AP-KGM/CS was 6:4, the adsorption of dyes (O56 and MB) reached the maximum at 364 mg/g and 425 mg/g, respectively. However, for the heavy metal

ions $Pb^{2+}$, $Cu^{2+}$ and $Cd^{2+}$, the adsorption capacity kept increasing slowly with increasing AP-KGM concentration. When the mass ratio is 8:2, the adsorption capacity of AP-KGM/CS aerogel to $Pb^{2+}$ increased by 20% compared with the one with mass ratio of 5:5. The regenerative property of the adsorbent is a very valuable factor in evaluating practicability of adsorbents (Ding et al. 2016). As shown in Fig. 6b, after five adsorption-desorption cycles of the AP-KGM/CS aerogel, the adsorption capacity of the adsorbents to the five pollutants only decreased slightly; more than 85% of the initial adsorption capacity was retained. The adsorption-desorption experiments of the AP-KGM/CS aerogel showed that AP-KGM/CS aerogel has excellent regeneration performance and AP-KGM plays an important role on adsorption process.

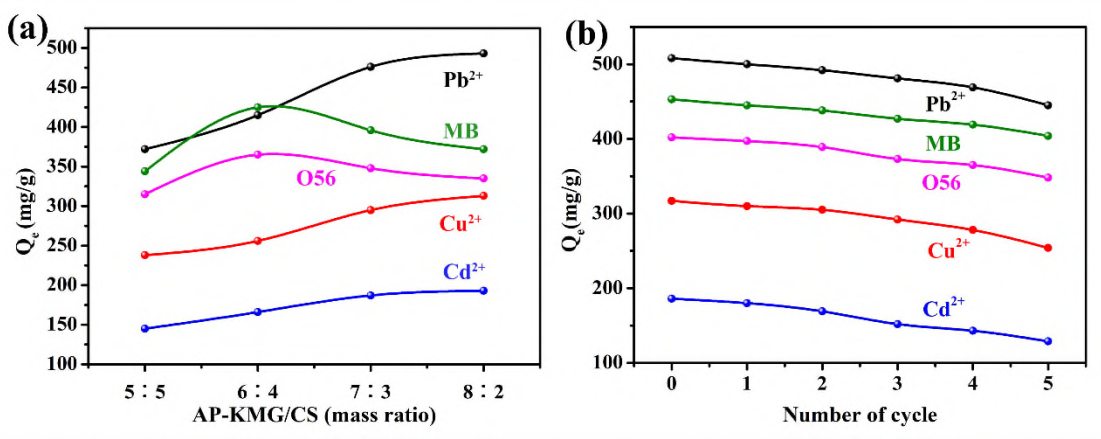


**Figure 6.** (a) The maximum adsorption capacities of AP-KGM/CS with different mass ratios to various pollutants. (b) Repeatability of as-prepared AP-KGM/CS aerogel after 5 cycles of repeated adsorption-desorption.

Adsorption is the result of a specific interaction between the adsorbent and the compound to be adsorbed. AP-KGM/CS aerogel exhibited a highly efficient adsorption to pollutants. The normalized remaining mass indicates that the pollutants@aerogel has

a different decomposition trend with the initial aerogel (Fig. S4). The amine groups and the carboxyl groups are easily ionized, which makes the AP-KGM/CS aerogel polycationic, and thus interacts with anionic derivatives, such as some dyes, through electrostatic interaction. The weakening of the carboxyl groups and amine groups after interaction with heavy metal ions also confirmed our analysis (Fig. S5). Furthermore, non-ionized groups have free electron pairs on the nitrogen atoms and may interact with electron-poor chemicals such as cations (Zhao et al. 2011). Although hydroxyl groups contribute to the binding of heavy metals in some studies, it is now generally accepted that metal binding occurs primarily on the amine and carboxyl groups. The hydroxyl group substantially contributes to stabilizing the binding of the metal ions onto the amine groups and the carboxyl groups. These reactive groups can bind heavy metal ions through various mechanisms such as complexation, chelation, ion exchange, and electrostatic adsorption. Apparently, the unique three-dimensional porous structure, high specific surface area and abundant surface active groups of the AP-KGM/CS aerogel ensure the high adsorption performance in pollution treatment, especially for the solutions including heavy metal ions and dyes.

Considering that most wastewater solutions in practice contain polymetallic situation rather than single metal ions, the influence of the presence of the multiple-cations on the adsorption capacity of the adsorbent is of great significance. Heavy metal adsorption not only depends on the properties of the adsorbent, but also on the nature of the metals involved and their competitive behavior on the adsorbent. In order to better understand the competitive adsorption behavior of $Pb^{2+}$, $Cu^{2+}$, and $Cd^{2+}$ in multi-

component solutions throughout the adsorption process, the equilibrium adsorption isotherm were carried out. Fig. 7 shows the kinetic curves of $Pb^{2+}$, $Cu^{2+}$, and $Cd^{2+}$ adsorption in mixed heavy metal solutions. The adsorption profiles of the three kinds of heavy metal ions followed the same trend. The adsorption kinetics of multi-component heavy metal ions was almost the same as that of heavy metal ions in single-component solution. The times for $Pb^{2+}$, $Cu^{2+}$, and $Cd^{2+}$ to reach equilibrium adsorption were 240 min, 150 min, and 70 min, respectively. In addition, the equilibrium adsorption capacities were 318 mg/g, 184 mg/g and 94 mg/g, respectively. The adsorption capacity of AP-KGM/CS aerogel has a significant enhancement in contrast with the AP-KGM powder (Fig. S6), as a result of improvement of amine group contents, hydrophilicity, and unique 3D networks. The chemical composition of the mixed heavy metal ions onto the adsorbents was analyzed by EDS (Figure S6). The proportion of tri-metal ions on the AP-KGM/CS aerogel was in agreement with the adsorption kinetics. Compared with the amount of equilibrium adsorption of single component heavy metal ions, the equilibrium adsorption of $Pb^{2+}$, $Cu^{2+}$, and $Cd^{2+}$ decreased by 32.2%, 27.6% and 34.7%, respectively. This mainly due to the limited adsorption sites in the adsorbent, which has led to the decrease.

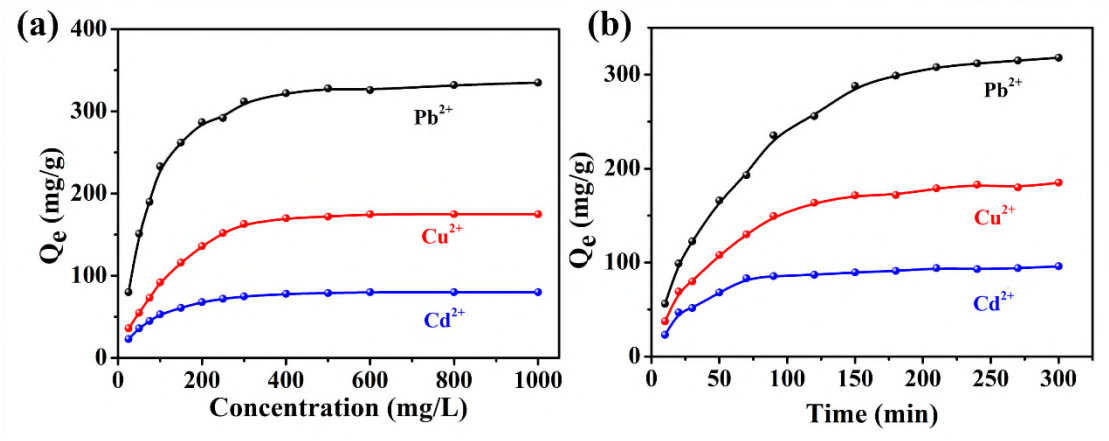


**Figure 7.** The adsorption isotherm curves of tri-metal ions onto AP-KGM/CS as a function of concentration (a) and time (b).

The results illustrate adsorption is in accord with the Langmuir isotherm model (Figure S7 and S8). When diverse metal ions compete for the same adsorption sites of adsorbents, metal ions with a lower affinity would be substituted by those with a greater affinity. According to the hydration radius of metal ions: $Pb^{2+}$ (0.401 nm), $Cu^{2+}$ (0.419 nm) and $Cd^{2+}$ (0.426 nm), $Pb^{2+}$ is more likely to reach the surface and be adsorbed compared to the other two heavy metal ions.

## Conclusion

In conclusion, we have fabricated the amphiphilic konjac glucomannan (AP-KGM) by chemical modification of KGM and its components containing both an anionic group and a cationic group. This unique amphoteric characteristic endows it with excellent adsorption ability to different types of pollutants. The konjac glucomannan was further used as the framework material, and chitosan was used as the shaping material to cross-link with glutaraldehyde to prepare aerogels via vacuum freeze-drying technology. The AP-KGM/CS aerogel exhibited a 3D network, high specific surface area, high porosity,

superior stability and abundant functional groups, which can be applied as a customized water remediation material. The saturated adsorption capacities of $Pb^{2+}$, $Cu^{2+}$, and $Cd^{2+}$ in mixed solutions were 318 mg/g, 184 mg/g and 94 mg/g, respectively. Moreover, such versatile strategy presented here can be extended to other functional hydro-/aerogel materials for promising applications.

**Acknowledgments**

The authors thank the National Natural Science Foundation of China (21501127 and 51502185), 111 Project (No. D17005), Nantong Science and Technology Project (GY12016030), Jiangsu Advanced Textile Engineering Center Project (Project No. SPPGO[2014]22), and the funds from the Priority Academic Program Development of Jiangsu Higher Education Institutions (PAPD). J. J. M and S. H. L contributed equally to this work.

**Reference:**

Ahmad T, Danish M (2018) Prospects of banana waste utilization in wastewater treatment: A review. J Environ Manage 206: 330-348.

Aragay G, Pons J, Merkoci A (2011) Recent Trends in Macro-, Micro-, and Nanomaterial-Based Tools and Strategies for Heavy-Metal Detection. Chem Rev 111: 3433-3458.

Bacelo HAM, Santos SCR, Botelho CMS (2016) Tannin-based biosorbents for environmental applications - A review. Chem Eng J 303: 575-587.

Bethke K, Palantoken S, Andrei V, Ross M, Raghuwanshi VS, Kettemann F, Greis K, Ingber TTK, Stuckrath JB, Valiyaveettil S, Rademann K (2018) Functionalized

Cellulose for Water Purification, Antimicrobial Applications, and Sensors. Adv Funct Mater 28: 1800409.

Chen PP, Zhang HP, Ding J, Lin XY, Lu X, Liu C, Tang Y (2017) Carboxylmethyl konjac glucomannan conjugated polydopamine composites for Pb(II) removal. Carbohydr Polym 162: 62-70.

Chuah TG, Jumasiah A, Azni I, Katayon S, Choong SYT (2005) Rice husk as a potentially low-cost biosorbent for heavy metal and dye removal: an overview. Desalination 175: 305-316.

Crini G, Badot PM (2008) Application of chitosan, a natural aminopolysaccharide, for dye removal from aqueous solutions by adsorption processes using batch studies: A review of recent literature. Prog Polym Sci 33: 399-447.

Dai XY, Zhang YY, Gao LN, Bai T, Wang W, Cui YL, Liu WG (2015) A Mechanically Strong, Highly Stable, Thermoplastic, and Self-Healable Supramolecular Polymer Hydrogel. Adv Mater 27: 3566-3571.

Dehghani MH, Sanaei D, Ali I, Bhatnagar A (2016) Removal of chromium(VI) from aqueous solution using treated waste newspaper as a low-cost adsorbent: Kinetic modeling and isotherm studies. J Mol Liq 215: 671-679.

Ding SY, Dong M, Wang YW, Chen YT, Wang HZ, Su CY, Wang W (2016) Thioether-Based Fluorescent Covalent Organic Framework for Selective Detection and Facile Removal of Mercury(II). J Amer Chem Soc 138: 3031-3037.

Ge YY, Li ZL (2018) Application of Lignin and Its Derivatives in Adsorption of Heavy Metal Ions in Water: A Review. ACS Sustain Chem Eng 6: 7181-7192.

Ho YS, Porter JF, McKay G (2002) Equilibrium isotherm studies for the sorption of divalent metal ions onto peat: Copper, nickel and lead single component systems. Water Air Soil Pollut. 141: 1-33.

Hu JS, Zhong LS, Song WG, Wan LJ (2008) Synthesis of hierarchically structured metal oxides and their application in heavy metal ion removal. Adv Mater 20: 2977-2982.

448 Huang RL, Qi W, Feng LB, Su, RX, He ZM (2011) Self-assembling peptide-
449 polysaccharide hybrid hydrogel as a potential carrier for drug delivery. Soft Matter
450 7: 6222-6230.
451 Huang W, Wang Y, Huang Z, Wang X, Chen L, Zhang Y, Zhang L (2018) On-Demand
452 Dissolvable Self-Healing Hydrogel Based on Carboxymethyl Chitosan and
453 Cellulose Nanocrystal for Deep Partial Thickness Burn Wound Healing. ACS
454 Appl. Mater. Interfaces 10: 41076-41088.
455 Katsuraya K, Okuyama K, Hatanaka K, Oshima R, Sato T, Matsuzaki K (2003)
456 Constitution of konjac glucomannan: chemical analysis and C-13 NMR
457 spectroscopy. Carbohydr Polym 53: 183-189.
458 Kim HN, Ren WX, Kim JS, Yoon J (2012) Fluorescent and colorimetric sensors for
459 detection of lead, cadmium, and mercury ions. Chem Soc Rev 41: 3210-3244.
460 Li SH, Huang JY, Mao JJ, Zhang LY, He CL, Chen GQ, Parkin IP, Lai YK (2019) In
461 vivo and in vitro efficient textile wastewater remediation by Aspergillus niger
462 biosorbent. 1: 168-176.
463 Liu Y, Wu P, Liu F, Li F, An X, Liu J, Wang Z, Shen C, Sand W (2019) Electroactive
464 Modified Carbon Nanotube Filter for Simultaneous Detoxification and
465 Sequestration of Sb (III). Environ Sci Technol 53: 1527-1535.
466 Liu YB, Li F, Xia Q, Wu JW, Liu JS, Huang MZ, Xie JP (2018) Conductive 3D sponges
467 for affordable and highly-efficient water purification. Nanoscale 10: 4771-4778.
468 Liu YB, Zheng YY, Du BW, Nasaruddin RR, Chen T, Xie JP (2017) Golden Carbon
469 Nanotube Membrane for Continuous Flow Catalysis. Ind Eng Chem Res 56: 2999-
470 3007.
471 Mao J, Ge M, Huang J., Lai Y, Lin C, Zhang K, Meng K, Tang Y (2017) Constructing
472 multifunctional MOF@rGO hydro-/aerogels by the self-assembly process for
473 customized water remediation. J Mater Chem A 5: 11873-11881.
474 Miao P, Tang YG, Wang L (2017) DNA Modified Fe3O4@Au Magnetic Nanoparticles
475 as Selective Probes for Simultaneous Detection of Heavy Metal Ions. ACS applied
476 materials & interfaces 9: 3940-3947.

Ngah WSW, Teong LC, Hanafiah M (2011) Adsorption of dyes and heavy metal ions by chitosan composites: A review. Carbohydr Polym 83: 1446-1456.

Pillai CKS, Paul W, Sharma, CP (2009) Chitin and chitosan polymers: Chemistry, solubility and fiber formation. Prog Polym Sci 34: 641-678.

Plamper FA, Richtering W (2017) Functional Microgels and Microgel Systems. Acc Chem Res 50: 131-140.

Si Y, Wang XQ, Yan CC, Yang L, Yu JY, Ding B (2016) Ultralight Biomass-Derived Carbonaceous Nanofibrous Aerogels with Superelasticity and High Pressure-Sensitivity. Adv Mater 28: 9512-9518.

Tahmasebi E, Masoomi MY, Yamini Y, Morsali A. (2015) Application of Mechanosynthesized Azine-Decorated Zinc(II) Metal-Organic Frameworks for Highly Efficient Removal and Extraction of Some Heavy-Metal Ions from Aqueous Samples: A Comparative Study. Inorg Chem 54: 425-433.

Tang YX, Gong DG, Lai YK, Shen YQ, Zhang YY, Huang YZ, Tao J, Lin CJ, Dong ZL, Chen Z. (2010) Hierarchical Layered Titanate Microspherulite: Formation by Electrochemical Spark Discharge Spallation and Application in Aqueous Pollutant Treatment, *J Mater Chem* 20: 10169-10178.

Wang B, Liao L, Huang Q, Cheng Y. (2011) Adsorption Behaviors of Benzonic Acid by Carboxyl Methyl Konjac Glucomannan Gel Micropheres Cross-Linked with $Fe^{3+}$. J Chem Eng Data 57: 72-77.

Wang S, Lu A, Zhang LN (2016) Recent advances in regenerated cellulose materials. Prog Polym Sci 53: 169-206.

Werber JR, Osuji CO, Elimelech M (2016) Materials for next-generation desalination and water purification membranes. Nat Rev Mater 1: 16.

Wu ZX, Zhao DY (2011) Ordered mesoporous materials as adsorbents. Chem Commun 47: 3332-3338.

You H, Jin YZ, Chen JC, Li CM (2018) Direct coating of a DKGM hydrogel on glass fabric for multifunctional oil-water separation in harsh environments. Chem Eng J 334: 2273-2282.

506 Yu CX, Shao ZC, Hou HW (2017) A functionalized metal-organic framework
507 decorated with O- groups showing excellent performance for lead(II) removal
508 from aqueous solution. Chem Sci 8: 7611-7619.
509 Zhang LY, Li XR, Wang MR, He YJ, Chai LY, Huang JY, Wang HY, Wu XW, Lai
510 YK (2016) Highly Flexible and Porous Nanoparticle-Loaded Films for Dye
511 Removal by Graphene Oxide-Fungus Interaction. ACS Appl Mater Interface 8:
512 34638-34647.
513 Zhang MY, Song LH, Jiang HF, Li S, Shao YF, Yang JQ, Li JF (2017) Biomass based
514 hydrogel as an adsorbent for the fast removal of heavy metal ions from aqueous
515 solutions. J Mater Chem A 5: 3434-3446.
516 Zhao GX, Li JX, Ren XM, Chen CL, Wang XK (2011) Few-Layered Graphene Oxide
517 Nanosheets As Superior Sorbents for Heavy Metal Ion Pollution Management.
518 Environ Sci Technol 45: 10454-10462.
519 Zhao QA, Li FY, Huang CH (2010) Phosphorescent chemosensors based on heavy-
520 metal complexes. Chem Soc Rev 39: 3007-3030.
521 Zhu WK, Cong HP, Yao HB, Mao LB, Asiri AM, Alamry KA, Marwani HM, Yu SH
522 (2015) Bioinspired, Ultrastrong, Highly Biocompatible, and Bioactive Natural
523 Polymer/Graphene Oxide Nanocomposite Films. Small 11: 4298-4302.
524 Zhu XY, Janczewski D, Guo SF, Lee SSC, Velandia FJP, Teo SLM, He T, Puniredd
525 SR, Vancso GJ (2015) Polyion Multi layers with Precise Surface Charge Control
526 for Antifouling. ACS Appl Mater Interface 7: 852-861.

527

528

**Supporting information**

# Robust amphiprotic Konjac Glucomannan Cross-linked Chitosan Aerogels for Efficient Water Remediation

**Jiajun Mao[a] · Shuhui Li[a,b] · Chenglin He[c] · Yuxin Tang[d] · Zhong Chen[e] · Jianying Huang[a*] · Yuekun Lai[a,c*]**

[a] College of Chemical Engineering, Fuzhou University, Fuzhou 350116, P. R. China

[b] Department of Chemistry, University College London, London, UK

[c] National Engineering Laboratory for Modern Silk, College of Textile and Clothing Engineering, Soochow University, Suzhou 215123, P. R. China

[d] Institute of Applied Physics and Materials Engineering, University of Macau, Macau, P. R. China

[e] School of Materials Science and Engineering, Nanyang Technological University, 50 Nanyang Avenue, Singapore

[*]Corresponding author

Corresponding author email: jyhuang@fzu.edu.cn; yklai@suda.edu.cn

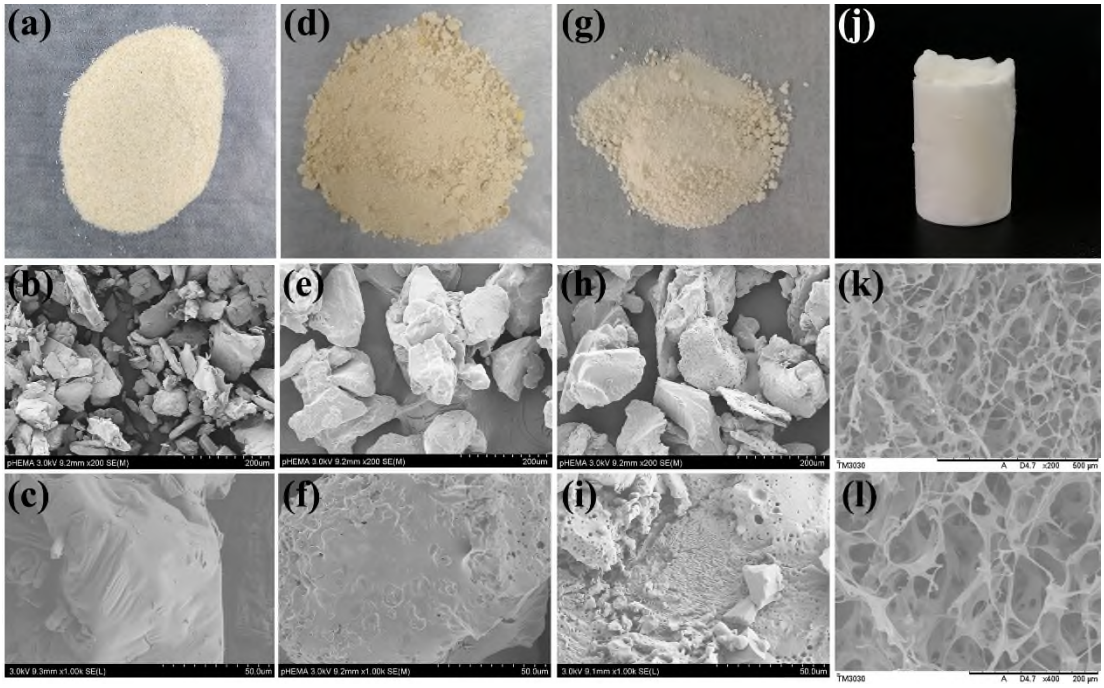


**Figure S1.** The optical images and the high/low resolution surface morphology of (a-c) KGM powder, (d-f) CM-KGM powder, (g-i) AP-KGM powder, and (j-l) AP-KGM aerogel.

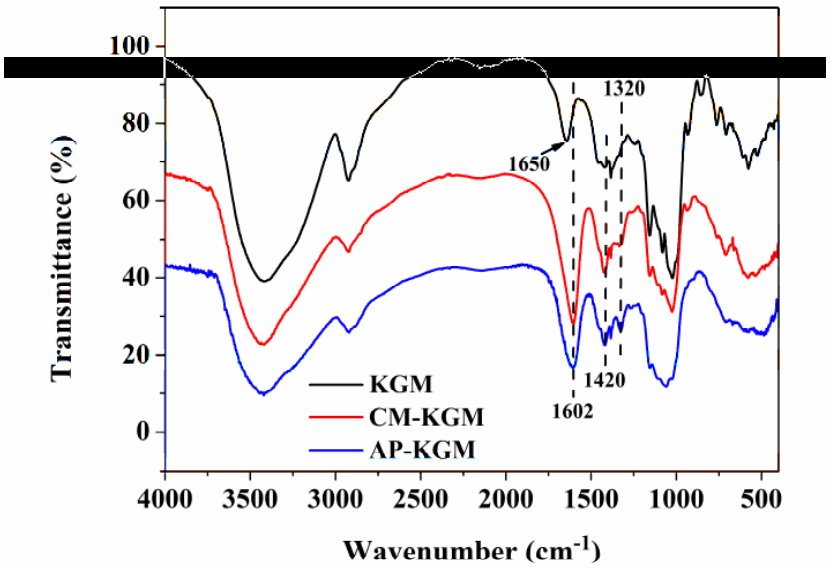


**Figure S2.** The FT-IR spectrum of the KGM, CM-KGM, AP-KGM.

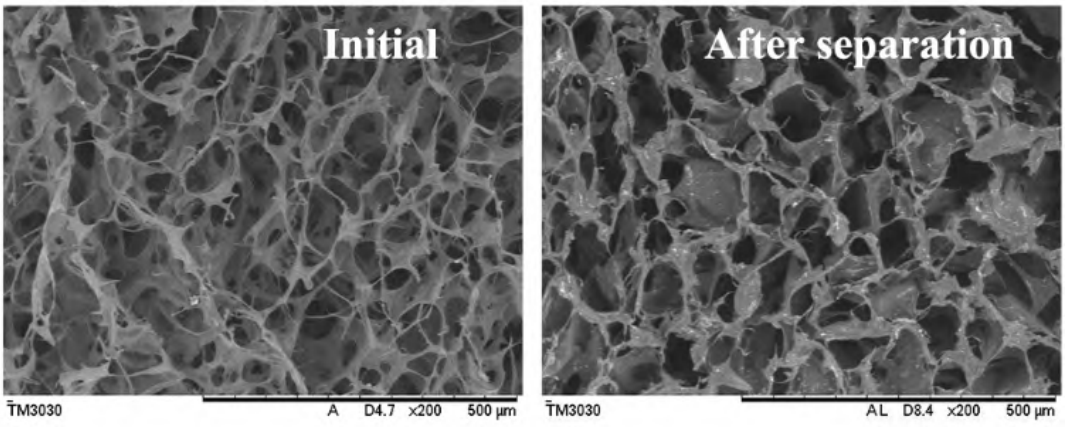


552

553 **Figure S3.** The SEM images of the aerogel before and after separation of heavy metal

554 ions.

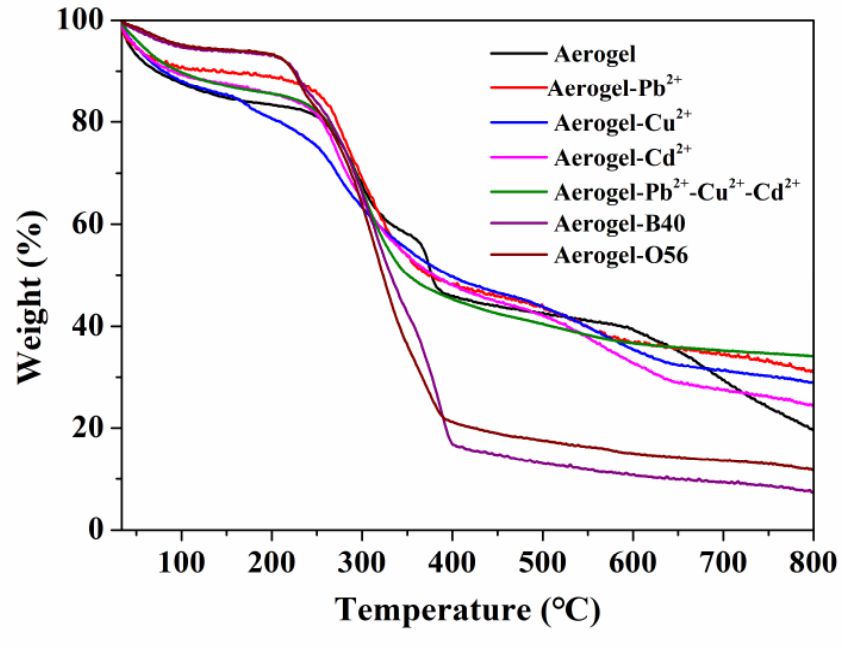


555

556 **Figure S3.** Normalized remaining mass of initial aerogel and diverse pollutants on

557 aerogels.

558

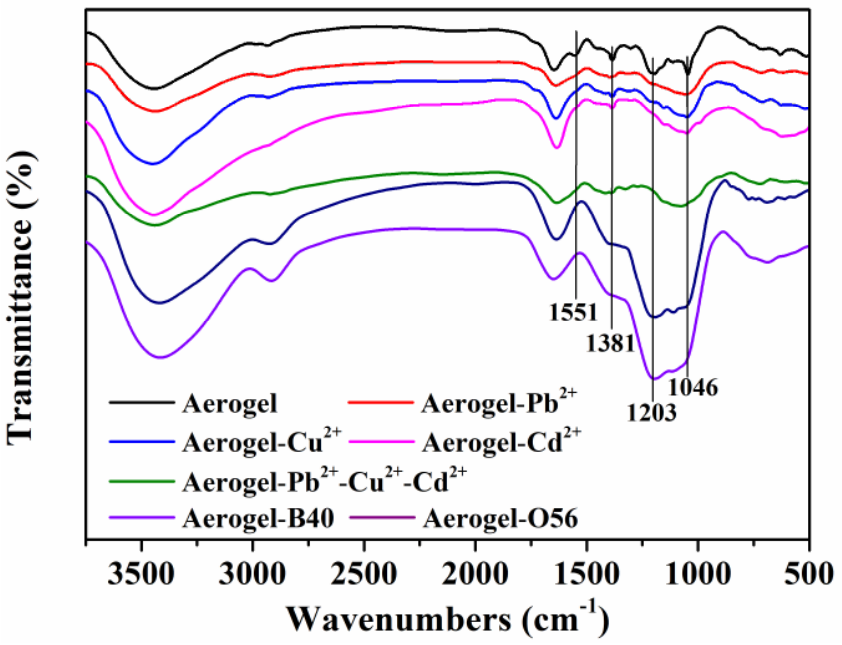


559

560 **Figure S4.** FT-IR spectrum of initial aerogel and diverse pollutants on aerogels.

561

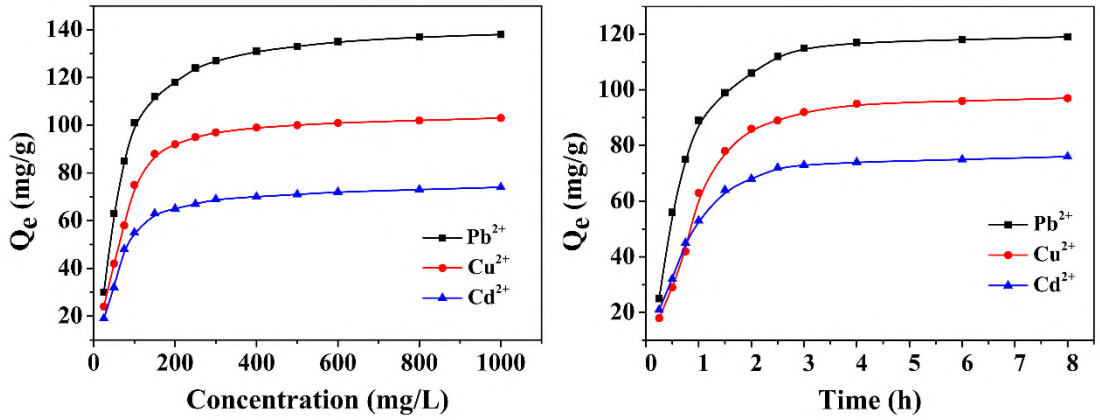


562

563 **Figure S5.** The adsorption isotherm curves of tri-metal ions onto AP-KGM as a

564 function of (left) concentration and (right) time.

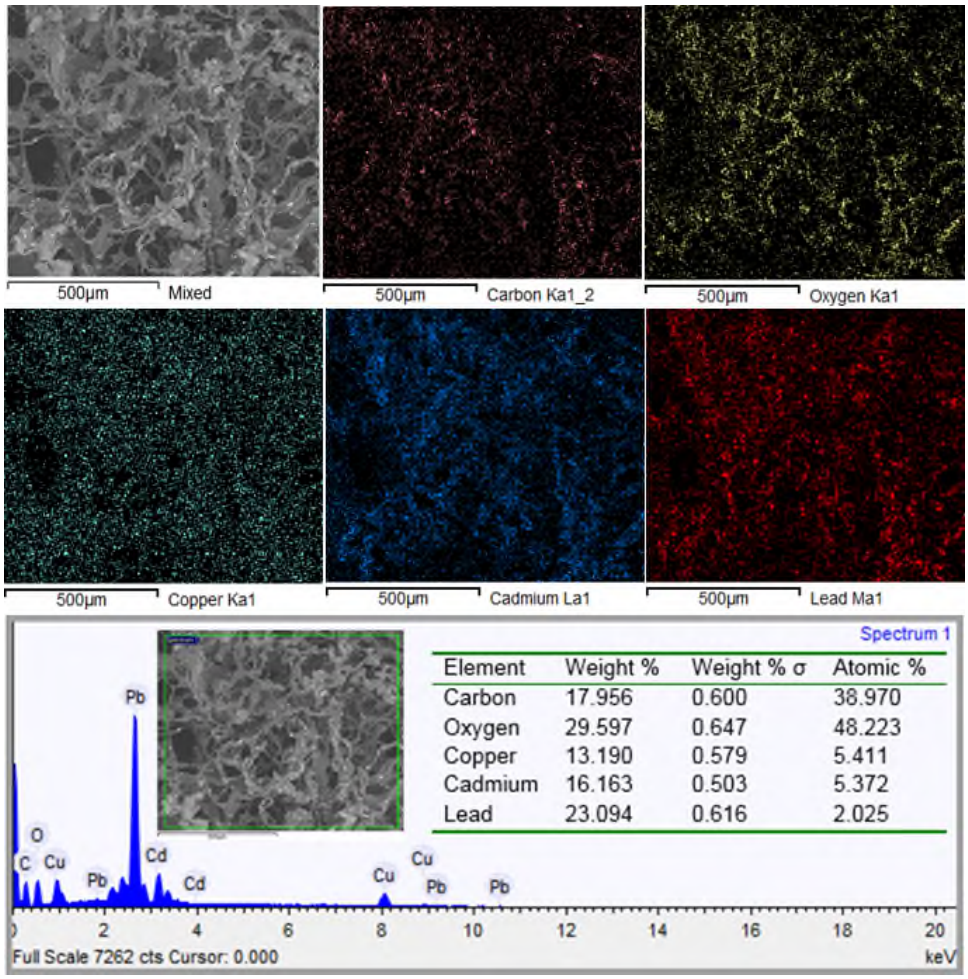


565

566 **Figure S6.** EDS patterns and mapping of mixed heavy metal ions onto AP-KGM/CS

567 aerogel.

568

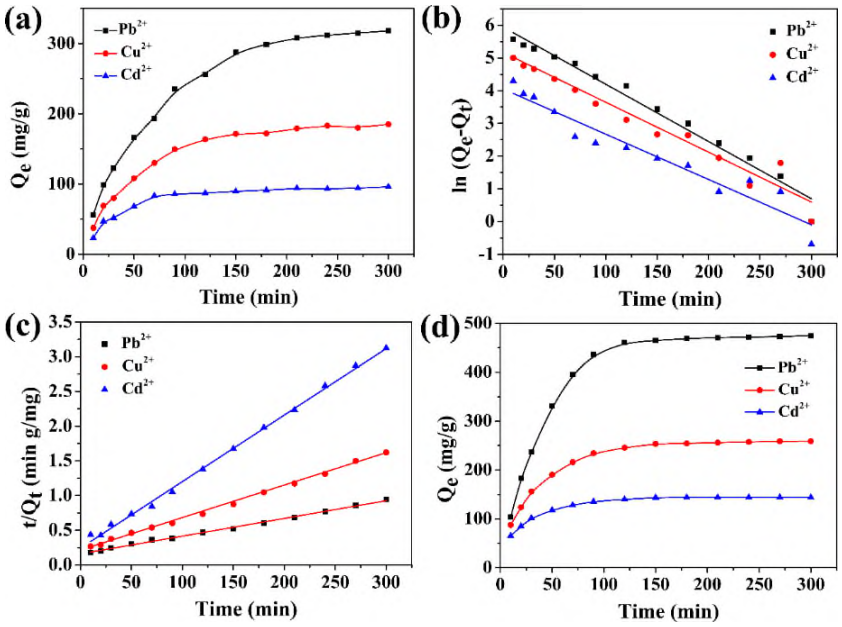


**Figure S7.** Adsorption capacity of ap-kgm /CS aerogel on mixed heavy metal ions (a) corresponding quasi-first-order adsorption kinetic model (b) and quasi-second-order kinetic model (c). (d) the adsorption capacity of heavy metal ions of in a single component solution with different concentrations.

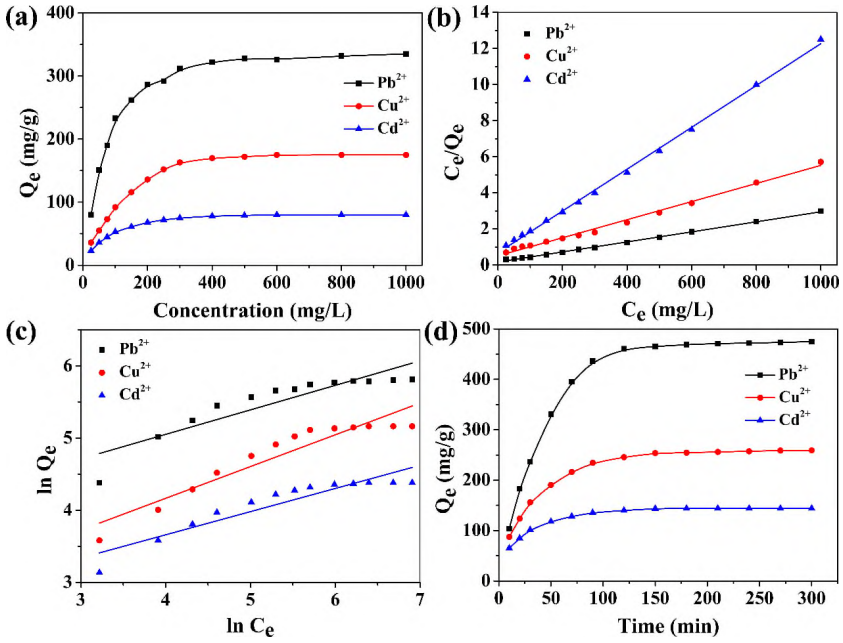


578

579 **Figure S8.** (a) The adsorption capacity of AP-KGM/CS aerogel on mixed heavy metal

580 ions, corresponding Langmuir adsorption isotherm model (b) and Freundlich

581 adsorption isotherm model (c). (d) The adsorption capacity of heavy metal ions of in a

582 single component solution with different concentrations.

583

584

585 **Table S1** Heavy metal ions and dyes removal efficiency comparison of aerogels

| **Materials** | **Heavy metal ions (single, mg $g^{-1}$)** | **Dyes (mg $g^{-1}$)** | **References** |
|---|---|---|---|
| PDA/rGA | N.A. | 89-360 | *Chem. Eng. J.* **2013**, 228, 468-481 |
| PDA/rGA | 100-320 | N.A. | *ACS Appl. Mater. Interface* **2013**, 5, 425-432 |
| α-FeOOH/rGA | 139-374 | N. A. | *ACS Nano* **2012**, 6, 2693-2703 |
| 4-HIFA (Indole aerogel) | 92-265 | N. A. | *J. Mater. Chem. A* **2019**, 7, 531-539 |
| Gelatin-based aerogel | 61.2 | 64.31-86.6 | *Chem. Eng. J.* **2019**, 358, 1539-1551 |
| Alginate/CNF aerogel | 300.61 | N. A. | *Cellulose* **2019**, 26, 903-916 |
| Waste paper/chitosan aerogel | 156.3 | N. A. | *Carbohyd. Polym.* **2018**, 193, 221-227 |
| **AP-KGM/Chitosan** | **144-469** | **267-348** | **This work** |

586